Design and Engineering of Amyloid Aggregation-Prone Fragments and Their Antimicrobial Conjugates with Multi-Target Functionality

Yanxian Zhang, Yijing Tang, Yonglan Liu, Dong Zhang, and Jie Zheng*

Amyloid aggregation and microbial infection are considered major risk factors for neurodegeneration and neuroinflammation in protein misfolding diseases (PMDs), including Alzheimer's disease (AD) and Type 2 diabetes (T2D). However, current amyloid inhibitors are mostly limited to single-target prevention strategies against specific amyloid proteins or pathogenic microbes, leading to no success for clinical cures of PMDs. Here, a step-by-step strategy to design new, multi-target amyloid aggregation-prone fragments (APFs) and their APFs antimicrobial agent conjugates is proposed, capable of achieving the stepwise improved multifunctionality of amyloid inhibition, antimicrobial activity, and amyloid imaging. The two APFs of KLVFF from A $oldsymbol{eta}$ (associated with AD) and FGAIL from hIAPP (associated with T2D) with β -structureforming property are selected and used as building block to construct a hybrid KLVFFGAIL peptide (K9) and a K9-AMC (7-amino-4-methylcoumarin) fluorescence conjugate, both of which have demonstrated the improved, multiple-target, sequence-independent functions to inhibit the aggregation of both A β and hIAPP, reduce both A β - and hIAPP-induced cell toxicity, prevent different microbial growth, and introduce fluorescence images for amyloid fibrils. The sequence-independent amyloid inhibition function of K9 and K9-AMC mainly stems from their cross-interactions with amyloid proteins via β -structure and aromatic interactions. This work provides a proof-ofconcept example to not only explore a new family of APFs as antimicrobial and anti-amyloid drugs for the therapeutic potential of PMDs, but also better understand the pathological links between protein aggregation and microbial infection in PMDs along the gut-brain axis.

1. Introduction

Abnormal protein aggregation and microbial infection are considered as major pathological risk factors for initiating and promoting the onset and progression of different protein misfolding diseases (PMDs), including Alzheimer's (AD), type 2 diabetes (T2D), and Parkinson's diseases (PD).^[1–3] While the exact pathological link between abnormal protein aggregation

Y. Zhang, Y. Tang, Y. Liu, D. Zhang, J. Zheng Department of Chemical, Biomolecular, and Corrosion Engineering The University of Akron Akron, OH, USA

E-mail: zhengj@uakron.edu

The ORCID identification number(s) for the author(s) of this article can be found under https://doi.org/10.1002/adfm.202102978.

DOI: 10.1002/adfm.202102978

and microbial infection is still largely unknown. "Amyloid cascade hypothesis" and "microbial infection hypothesis" have driven different prevention and treatment strategies to design i) amyloid inhibitors for preventing amyloid aggregation and ii) antibiotics for preventing microbial infection, [4-6] most of which do not achieve any clinical success. Due to the multifactorial nature of PMDs, single-target prevention strategies provide marginal benefits for amyloid inhibition and medical treatments. Therefore, it is highly important, but a great challenge for developing a new multiple-target amyloid model that can re-examine or reconcile the two hypotheses for better understanding pathological causes and links of PMDs.

While full-length amyloid proteins are reported to misfold and aggregate into insoluble amyloid fibrils that are pathologically linked to PMDs, it is generally accepted that only aggregation-prone fragments (APFs) play a determinative role in driving full-length amyloid peptides to self-assemble into β -structure-rich amyloid fibrils. A number of APFs have been identified from different full-length amyloid proteins, including KLVFF and GLM-VGGVVIA from amyloid- β (A β , associated with AD), [7] NFGAILS and LANVFLVH

from human islet amyloid polypeptide (hIAPP, associated with T2D), [8] VQIVYK from tau protein (associated with AD), [9] and QVLHTSN from β_2 -microglobulin ($\beta 2$ m, associated with hemodialysis-associated amyloidosis). [10] Despite the high sequence diversity of these APFs, they all contain hydrophobic-dominant residues responsible for amyloid aggregation. More importantly, due to β -structure-forming property, APFs may serve as a sequence/structural template to design general amyloid inhibitors via a "like-interacts-like" mechanism, [11] that is, APFs with β -structure-forming properties will highly likely interact with conformationally similar β -structures of amyloid proteins, which will competitively reduce amyloid-amyloid interactions, thereby preventing amyloid aggregation. [12–14]

Apart from a general amyloid inhibition property, a number of our and other studies have shown that some amyloid proteins (e.g., $A\beta^{[15,16]}$ hIAPP,^[17] and Serum amyloid A [^{18]}) and APFs (e.g., $PrP_{23-231}^{[19]}$ and GNNQQNY^[1,20]) possess





www.afm-iournal.de

antimicrobial activity against several common microorganisms with a potency equivalent to, and in some cases greater than, LL-37 antimicrobial peptide. [18,19,21-26] Such antimicrobial property has been explored to enlighten a new class of antifouling/antibacterial materials, as derived from amyloid-like protein aggregates, for effectively achieving both interfacial anchoring and antifouling capability. [27-30] The "microbial infection hypothesis" suggests that microbial infection promotes the overexpression, accumulation, and aggregation of amyloid proteins, which in turn triggers the neuroinflammation and neurodegeneration of PMDs. [31-33] Several compounds (e.g., Masitinib, COR388, and ALZT-OP1a/OP1b) targeting microbial infection have been progressed to phase 3 clinical trials for PMD treatments.[34] The potential link between amyloid aggregation and microbial infection also suggests that conventional singletarget prevention strategies against either amyloid proteins or microbes have proven insufficient. Instead, developing new inhibitors targeting both amyloid proteins and microbes may open new possibilities for better understanding of the pathogenetic role of amyloid proteins or microbes in PMDs and for the development of effective treatments for PMDs.

In this work, we proposed a new step-by-step strategy to rationally design new APFs and APFs-fluorescent conjugates with β -structure-forming property, which serve as multi-target inhibitors to prevent both microbial infection of Staphylococcus aureus and Staphylococcus epidermidis and amyloid aggregation of $A\beta$ (associated with AD) and hIAPP (associated with T2D). Our design strategy is based on the two rationales to select two APFs of KLVFF from A β and FGAIL from hIAPP: i) A β and hIAPP have been reported to share high structure/sequence similarity, cross-interact with each other to form hybrid amyloid fibrils, and co-exist in bloods and cerebrospinal fluids, [35] which may explain the AD-T2D link as observed in clinical data, [36] and ii) KLVFF and FGAIL themselves can form β -structurerich amyloid-like fibrils, similar to their parent $A\beta$ and hIAPP. Thus, it is expected that KLVFF and FGAIL will interact with their parent proteins via conformationally specific β -structure interactions. To further optimize our design, we first combined KLVFF and FGAIL sequences into KLVFFGAIL (K9) to enhance cross-interaction ability to both A β and hIAPP and their dual amyloid inhibition against $A\beta$ and hIAPP aggregation. Then, we conjugated 7-amino-4-methylcoumarin (AMC) to the C-terminus of K9 to produce a hybrid K9-AMC, which is expected to enhance antimicrobial activity, because AMC[37] as a coumarin fluorescence derivative is a well-demonstrated antimicrobial compound with strong antibacterial and antifungal activities^[38] and antioxidant and anticancer properties. [39,40] Additionally, the aromatic nature of AMC allows increasing hydrophobic and π - π interactions between AMC and amyloid proteins. Through this step-by-step design strategy, we demonstrated the stepwise improvement of multifunctionality of the APFs from KLVFF and FGAIL to K9 to K9-AMC, including the enhanced i) amyloid inhibition efficiency against both A β and hIAPP aggregation and toxicity, ii) antimicrobial activity against different bacteria, and iii) fluorescent characteristics for in vivo imaging. This work for the first time provides a new peptide and peptide-conjugate system as multi-target inhibitors to prevent both microbial infection and amyloid aggregation pathologically linked to PMDs.

2. Results and Discussion

We proposed a step-by-step strategy to re-design and repurpose KLVFF from A β and FGAIL from hIAPP for achieving new and multi-target amyloid inhibitors. A key design principle to select KLVFF and FGAIL as basic building blocks is based on two fundamentals: i) both $A\beta$ and hIAPP can cross-interact with each other to form fibrillar co-assembly^[41] and ii) both KLVFF from $A\beta$ and FGAIL from hIAPP is derived from high hydrophobic amyloid region (Figure 1a), and exhibit the self-assembling property to form amyloid-like fibrils similar to those formed by full-length A β and hIAPP.^[42] To achieve this goal, both KLVFF and FGAIL were combined into KLVFFGAIL (K9) for realizing the cross-interactions with both A β and hIAPP to prevent their aggregations. Next, the C-terminus of the K9 peptide was modified with aromatic AMC moiety (K9-AMC) to amplify its antimicrobial activity (Figure 1b). Most importantly, all these short peptides of KLVFF, FGAIL, K9, and K9-AMC were able to self-assemble into amyloid-like fibrils (Figure 1c). Among them, K9-AMC outperformed others in terms of anti-amyloid aggregation, antimicrobial activity, and fluorescent signals for imaging $A\beta$ and hIAPP aggregates.

2.1. Dual Inhibition Effect of K9 on the Aggregation and Toxicity of Both $A\beta$ and hIAPP

As a control for comparison, we first examined the inhibitory property of KLVFF and FGAIL against the aggregation of both $A\beta$ (associated with AD) and hIAPP (associated with T2D) in vitro using ThT, atomic force microscopy (AFM), and CD. As shown in Figure 2a, KLVFF showed concentration-dependent inhibition against A β aggregation, as evidenced by the reduction of final ThT intensity from 440 to 405 a.u. and from 440 to 300 a.u (equivalent to 8% to 32% of A β fibrillization reduction) as KLVFF:A β molar ratio increased from 1:1 to 4:1. But KLVFF also inhibited hIAPP aggregation by 20% at all KLVFF: hIAPP ratios, showing a nearly dose-independent inhibition behavior. Similarly, FGAIL (100 µM) demonstrated its cross-interaction ability to both A β and hIAPP, thus leading to a maximal A β and hIAPP inhibition of 35% and 31%, respectively. Next, upon combining KLVFF and FGAIL into a nine-residue peptide of K9, K9 exhibited the much higher amyloid inhibition property than individual KLVFF and FGAIL in a dose-dependent manner, that is, as K9:amyloid molar ratios increased from 1:1 to 4:1, A β fibrillization was reduced by 29–97%, while hIAPP fibrillization was reduced by 16-39%.

In parallel, visual inspection of such inhibition effect was also demonstrated by AFM images. It can be seen in Figure 2b that upon incubation of amyloid peptides (A β and hIAPP) with APFs of 100 μ M (KLVFF, FGAIL, and K9) for 24 h, all APFs inhibited amyloid fibril formation to some extent, as compared to the densely formed A β and hIAPP fibrils alone. Particularly, both K9 and FGAIL displayed higher inhibition efficiency than KLVFF, that is, addition of APFs in freshly prepared amyloid solution almost eliminated the formation of mature fibrils, instead only a small amount of nonfibrillar spherical aggregates were observed. Furthermore, we quantified the structural transition and misfolding of A β and hIAPP (25 μ M) in the presence

www.afm-journal.de

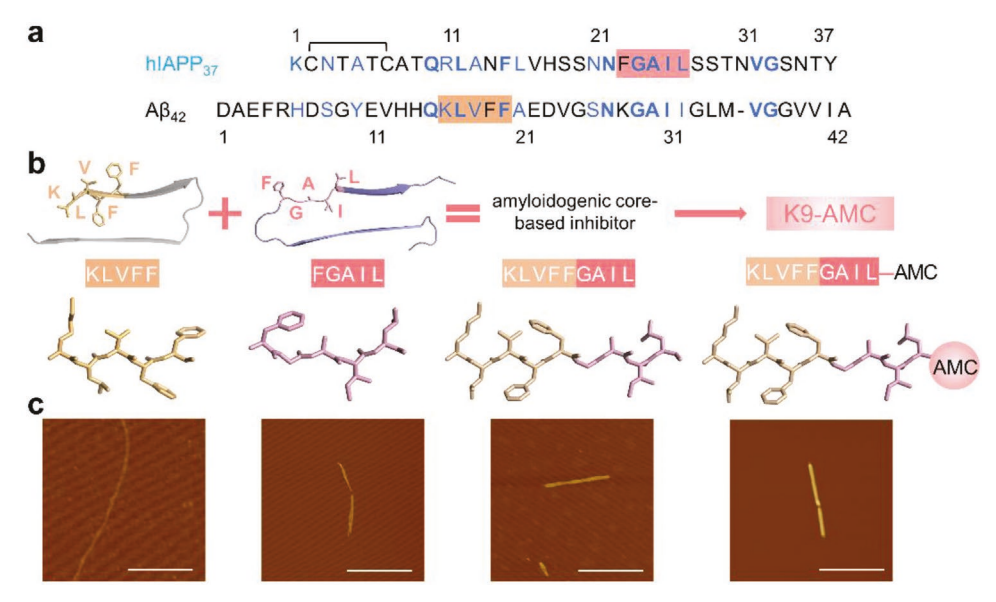


Figure 1. Rational design and repurpose of APF peptides and peptide-conjugate as multi-target amyloid inhibitors. a) Sequence comparison of full-length $A\beta$ and hIAPP proteins. (blue: similar residues; bold: identical residues; highlight: amyloid APFs). b) Step-by-step design of APFs from KLVFF from $A\beta$ and FGAIL from hIAPP to K9 to K9-AMC to achieve multi-target functionality. c) Self-assembly of APFs (2 mM) into amyloid-like fibrils after 5 days incubation in physiological environment (pH 7.4, 37 °C) by AFM. Scale bars = 1μm.

of different APFs (25-100 µM) using time-dependent circular dichroism (CD). As controls, Figure S1, Supporting Information, showed that KLVFF aggregation led to two major positive maxima at 200 nm corresponding to π - π * transition and at 216 nm corresponding to a $n-\pi^*$ transition. Differently, FGAIL was lack of the typical secondary structure, instead it just presented random structure as evidenced by a dominate negative peak at ≈190 nm. Similarly, K9 also displayed a small negative peak at 190 nm, indicating the presence of a random secondary structure. Another set of controls in Figure S2, Supporting Information, showed that both A β and hIAPP (25 μ M) alone displayed a typical structural transition, starting from random coli as signified by negative peak at \approx 198 nm, to α -helix (negative peak at ≈208 nm and ≈222 nm), finally to characteristic cross β -sheet structure (negative peak at \approx 215 nm). For comparison, when co-incubation of KLVFF with A β or hIAPP at 4:1 ratio, the β -structure formation of A β or hIAPP was largely disrupted due to the increase of aromatic stacking interactions between KLVFF and amyloid peptides. Similarly, FGAIL also suppressed the structural transition of A β or hIAPP from random coils at 190 nm to β -structures at 195 and 220 nm. Evidently, K9 indeed demonstrated a concentration-dependent dual inhibition ability to delay the spectral change (i.e., secondary structure change) of $A\beta/hIAPP$ (Figure S2b,e, Supporting Information). However, final β -sheet structure content of K9/ amyloid systems was slightly higher than KLVFF/amyloid systems and comparable to FGAIL/amyloid systems (Figure S2c,f, Supporting Information). This indicates that K9 still exhibit high inhibition ability to prevent the growth and association of amyloid aggregates into amyloid fibrils (as indicated by strong ThT intensity reduction in Figure 2a), but it is less efficient to alter the preformed β -structures in these amyloid aggregates. In other words, it is possible for K9 to inhibit $A\beta$ and hIAPP fibrillization by forming off-pathway oligomeric complexes,

whose β -structures are largely retained and not disrupted by K9. Meanwhile, as shown in Figure S1, Supporting Information, native K9 (26%+24% = 50% β -sheet structure) possessed the higher β -sheet structure than KLVFF and FGAIL (20% and 22% β -sheet structure), which may also contribute to the final high β -structure content in the A β /hIAPP-K9 complex.

We further examined whether all APFs could protect cells from A\beta- and hIAPP-induced toxicity using MTT assay, where SH-SY5Y cells and RIN-m5F cells were used to assess the AB- and hIAPP-induced cytotoxicity, respectively. As a control. all KLVFF, FGAIL, and K9 were almost non-toxic to SH-SY5Y and RIN-5fm cells (97.4–115.9% cell viability at 25–100 μM concentration), except the notable toxicity of KLVFF to RIN-m5F cells at 100 μ M concentration (82.4% cell viability). While A β and hIAPP (25 µM) alone significantly decreased cell viability to 52.6% (0 h freshly prepared) and 61.5% (20 h aged), and 64.1% (0 h freshly prepared) and 65.6% (20 h aged), respectively (Figure 2c,d). When introducing KLVFF, FGAIL or K9 to $A\beta$ -cultured SH-SY5Y cells, they all exhibited a concentrationdependent cell protection, as evidenced by the increase of cell viability from 61.5% to 79.8% with KLVFF, 77.6% with FGAIL, and 83.9% with K9 (Figure 2c). However, three APFs did not show obvious cell protection from hIAPP-induced cell toxicity. As shown in Figure 2d, maximum cell viability was 65.6%, 67.9%, 62.4%, and 67.4% in the presence of hIAPP, hIAPP and KLVFF, hIAPP and FGAIL, and hIAPP and K9, respectively. It should be noted that due to complex pathological nature of amyloids, the inhibition of amyloid aggregation and amyloid toxicity may not necessarily be correlated with each other. It is not surprising that KLVFF derived from A β may not have direct cell protection effect on hIAPP-relevant RIN-m5F cells. While FGAIL as a hIAPP fragment can inhibit hIAPP aggregation, it is also possible that FGAIL redirects the aggregation pathway of hIAPP into different FGAIL-hIAPP aggregates, which may

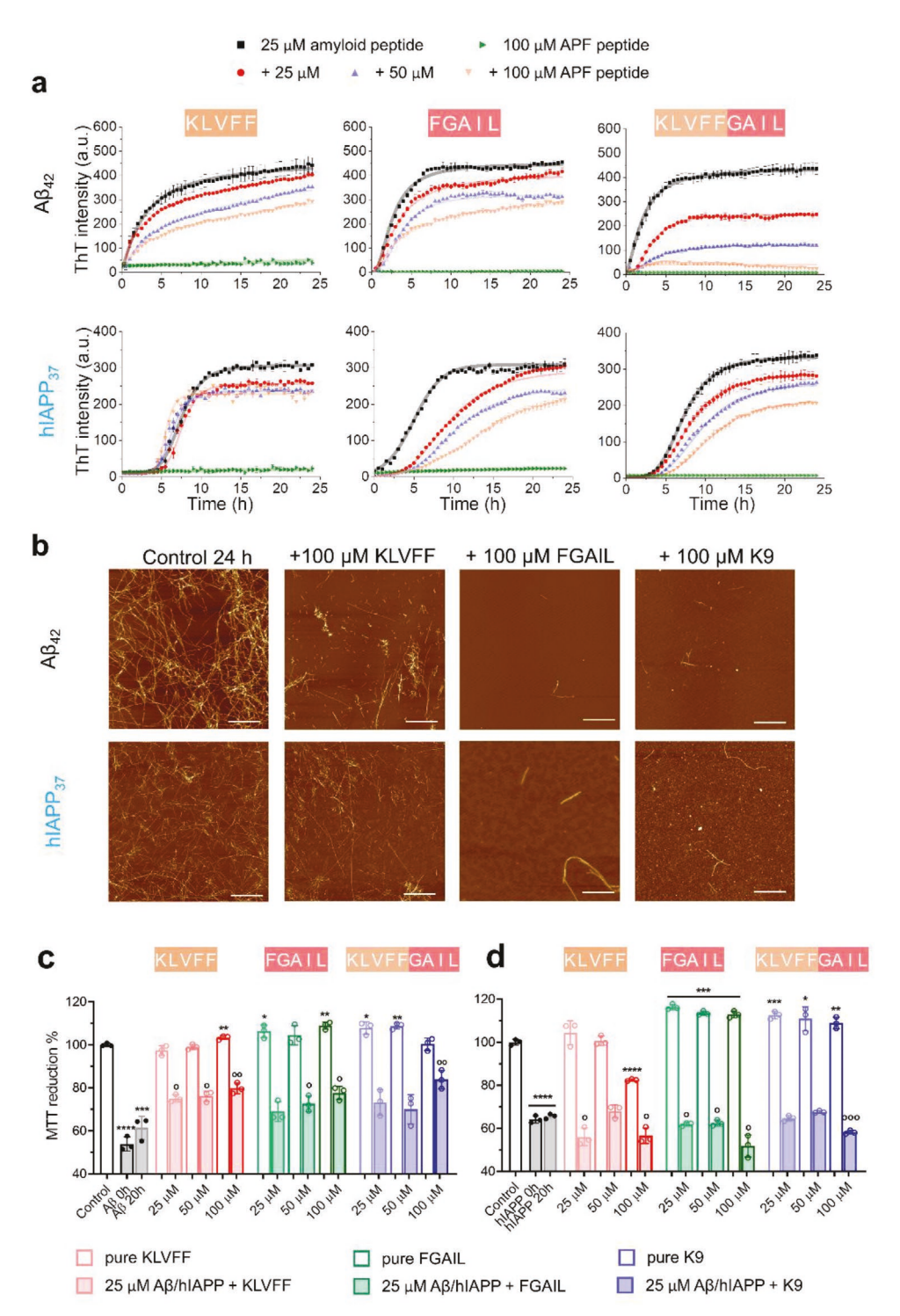


Figure 2. Dual amyloid inhibition activities of KLVFF, FGAIL, and K9. a) ThT kinetic aggregation profiles to quantify the inhibition of A β (25 μM) or hIAPP (25 μM) in the absence (black) or presence of KLVFF, FGAIL, and K9 at different concentrations (25–100 μM). All data represent mean \pm standard error of triplicate measurements. b) AFM images of A β (25 μM) or hIAPP (25 μM) aggregates in the absence or presence of 100 μM KLVFF, FGAIL, and K9. All samples are imaged after 24 h incubation under physiological conditions (pH 7.4, 37 °C). Scale bars = 1 μm. Dose-dependent inhibition effect of KLVFF, FGAIL, and K9 on c) A β -, and d) hIAPP-induced cellular toxicity by MTT assay. Statistical analysis (n = 3) is conducted for cells treated with APFs, A β , or hIAPP alone relative to control (*, p < 0.05; ***, p < 0.01; ****, p < 0.001; ****, p < 0.001), as well as cells treated with both APFs and A β or hIAPP relative to cells treated with A β or hIAPP alone (°, p < 0.05; °°, p < 0.01; °°°, p < 0.001).

or may not be cytotoxicity to RIN-m5F cells. Similarly, K9 had a weak protection effect on cell viability, and this is in accordance with the above explanation that K9 and hIAPP can form a

diverse of hybrid aggregates with or without enhanced cytotoxicity. Taken together, our findings provide preliminary evidence to support our hypothesis that i) APFs containing β -structure





www.afm-iournal.de

show a sequence-independent inhibition ability to prevent the misfolding and aggregation of $A\beta$ and hIAPP via the suppression of β -structure formation; ii) Cross-interactions of APFs with amyloid protein determines their inhibition efficacy and inhibition pathways; iii) hybrid APF-amyloid aggregates might have varied cell cytotoxicity, which are hypothetically associated with the degree of aggregation and oligomerization.^[43]

2.2. Enhanced Dual Amyloid Inhibition Activity of AMC-K9

Upon demonstrating the dual inhibition activity of both $A\beta$ and hIAPP aggregation, K9 also suffers from low inhibition efficiency against hIAPP aggregation and amyloid-induced cell toxicity. To overcome this issue, we optimized the K9 by adding AMC to its C-termini, given that, i) AMC with aromatic structure is expected to enhance its binding affinity to amyloid peptides via hydrophobic and π - π interactions, so as to prevent the self-aggregation of amyloid peptides, ii) AMC as a natural coumarin derivative has been recognized with its antimicrobial, antioxidant, anti-inflammatory, and anti-cancer properties, [38–40] and iii) AMC as a fluorescent molecule exhibits a maximal excitation at 365 nm and emission at 440 nm, which is used for detecting and imaging amyloid aggregates (Figure 3a). Herein, we firstly evaluated the optical property of K9-AMC. Figure 3b showed that K9-AMC in water solution exhibited a maximal excitation at 337 nm and a wide emission region of 350-500 nm and a maximal peak at 393 nm. Consistently, ThT fluorescent assay showed the self-assembly behavior of K9-AMC alone at the concentrations of 12.5 µM or above (Figure 3c). Such self-aggregation property of K9-AMC is likely attributed by its aromatic chemistry, in sharp contrast to the lack of any self-aggregation behavior of KLVFF, FGAIL, and K9 even at concentration of 100 µM (Figure 2a). Considering the existence of aromatic and hydrophobic residues in K9-AMC and amyloid peptides, we firstly quantitively analyzed the binding affinity of K9-AMC to A β and hIAPP using fluorescence titration. The titration of K9-AMC (0.2 μM) with the increased amount of $A\beta$ and hIAPP from 0.2 to 17 μ M was performed, during which the excess of both $A\beta$ and hIAPP resulted in a new fluorescence emission maximum at 440 nm (Figure 3d). Specifically, the slight decrease of fluorescence intensity at 390 nm can be attributed to the quenching effect as induced by hydrophobic interactions between amyloid A β /hIAPP and K9-AMC.[44] Meanwhile, the strong red-shift of emission, as indicated by the increasing emission peak intensity at 440 nm, further emphasizes the enhancement effect of charge transfer from amyloid A β /hIAPP (donor) to K9-AMC (acceptor) via intermolecular bindings. [45,46] Different from small fluorescence quenching at 390 nm, fitting fluorescence titrations by taking into account of strong emission at 440 nm allows to better estimate charge transfer between A β /hIAPP and K9-AMC through strong intermolecular interaction.^[46] By recording the fluorescence intensity increased at 440 nm with titration, the binding affinities (K_D) were determined, through the simplified 1:1 binding model, [14,47] as 240.6 \pm 1.6 nM and 307.9 \pm 1.9 nM between K9-AMC-A β and K9-AMC-hIAPP, respectively (Figure 3e). Of note, since the freshly prepared K9-AMC, $A\beta$, and hIAPP mainly consist of monomers, fluorescence titration

results demonstrate a nanomolar binding affinity of K9-AMC to monomeric A β and hIAPP. Further, we also observed high binding affinity of K9-AMC (10 µM, freshly prepared) to mature $A\beta$ and hIAPP fibrils, accompanied by a strong fluorescence emission to image A β and hIAPP fibrils (Figure 3f). Given that i) AMC molecule (10 μ M) alone failed to bind and imaging A β and hIAPP fibrils as demonstrated in Figure S3a, Supporting Information, ii) Co-incubation of K9-AMC monomers with A β and hIAPP monomers did not produce any immediate fluorescence (Figure S3b, Supporting Information), and iii) K9-AMC alone can self-assemble into short, thick fibrils (1 mM, 48 h, 37 °C) with strong fluorescence emission (Figure S3c, Supporting Information), the fluorescent imaging of the preformed A β and hIAPP fibrils by freshly prepared K9-AMC monomers is solely stemmed from K9-AMC binding to A β and hIAPP fibrils, not from K9-AMC itself (Figure S3d, Supporting Information).

High binding affinity between K9-AMC and A β /hIAPP is expected to competitively interfere with $A\beta$ - $A\beta$ and hIAPPhIAPP interactions, thus achieving its amyloid inhibition property. To evaluate the inhibition activity of K9-AMC against A β and hIAPP aggregations, ThT data in Figure 4a showed that K9-AMC of 12.5 μ M (0.5 molar equivalent to A β) reduced A β fibrilization by 64%. Further increase of K9-AMC to 25 μM led to \approx 95% decrease of A β fibrilization. However, no further enhanced A β inhibition was observed as K9-AMC concentration was above 25 μ M, suggesting that 25 μ M of K9-AMC is an optimal concentration to achieve the high inhibition efficacy against $A\beta$ fibrillization. In the case of K9-AMC and hIAPP, K9-AMC also exhibited the dose-dependent hIAPP inhibition efficacy, that is, K9-AMC-induced hIAPP inhibition increased from 19% at \leq 25 μ M to \approx 33% at 50 μ M to \approx 56% at 100 μ M. ThT data in Figure 4a clearly showed that AMC alone did not exhibit any inhibition effect on the aggregation of both A β and hIAPP, while K9 alone at equimolar ratio to amyloid peptides reduced the aggregation of A β by 29% and hIAPP by 16% (Figure 2a). Upon introducing AMC to the C-terminal of K9 (i.e., K9-AMC), K9-AMC at equimolar ratio can reduce the aggregation of A β by 95% and hIAPP by 19% (Figure 4a). Evidently, such enhanced inhibition effect of K9-AMC, in comparison with both K9 and AMC, is likely stemmed from the synergistic conjugation of K9 with AMC to enhance hydrophobic and aromatic interactions with amyloid peptides. Such synergetic effects became more pronounced at the higher molar ratios of K9-AMC:amyloid > 1. Furthermore, CD spectra was used to monitor the structural transition of A β and hIAPP (25 μ M) in the presence of K9-AMC (25-100 μM). As a control, K9-AMC (100μM) alone displayed a typical structural transition, starting from α -helical structure^[48] as signified by a strong positive peak at 200 nm and two negative peaks at 216 and 230 nm at 0 h to characteristic β -sheet structure as indicated by a stronger minimum at 216 nm and a decreased peak at 200 nm (Figure S4a, Supporting Information). For comparison, when K9-AMC was added to $A\beta$ fresh solution at a molar ratio of 1:1 to 4:1, CD spectra differences between the A β /K9-AMC mixture and pure A β spectra confirmed the interactions between A β and K9-AMC (Figures S4b, Supporting Information). Specifically, A β /K9-AMC mixture displayed an amplified signal at 200 nm within 6 h, suggesting a π - π * transition of β -turn due to the binding of K9-AMC.^[49,50] In parallel, hIAPP/K9-AMC mixture presented the structural

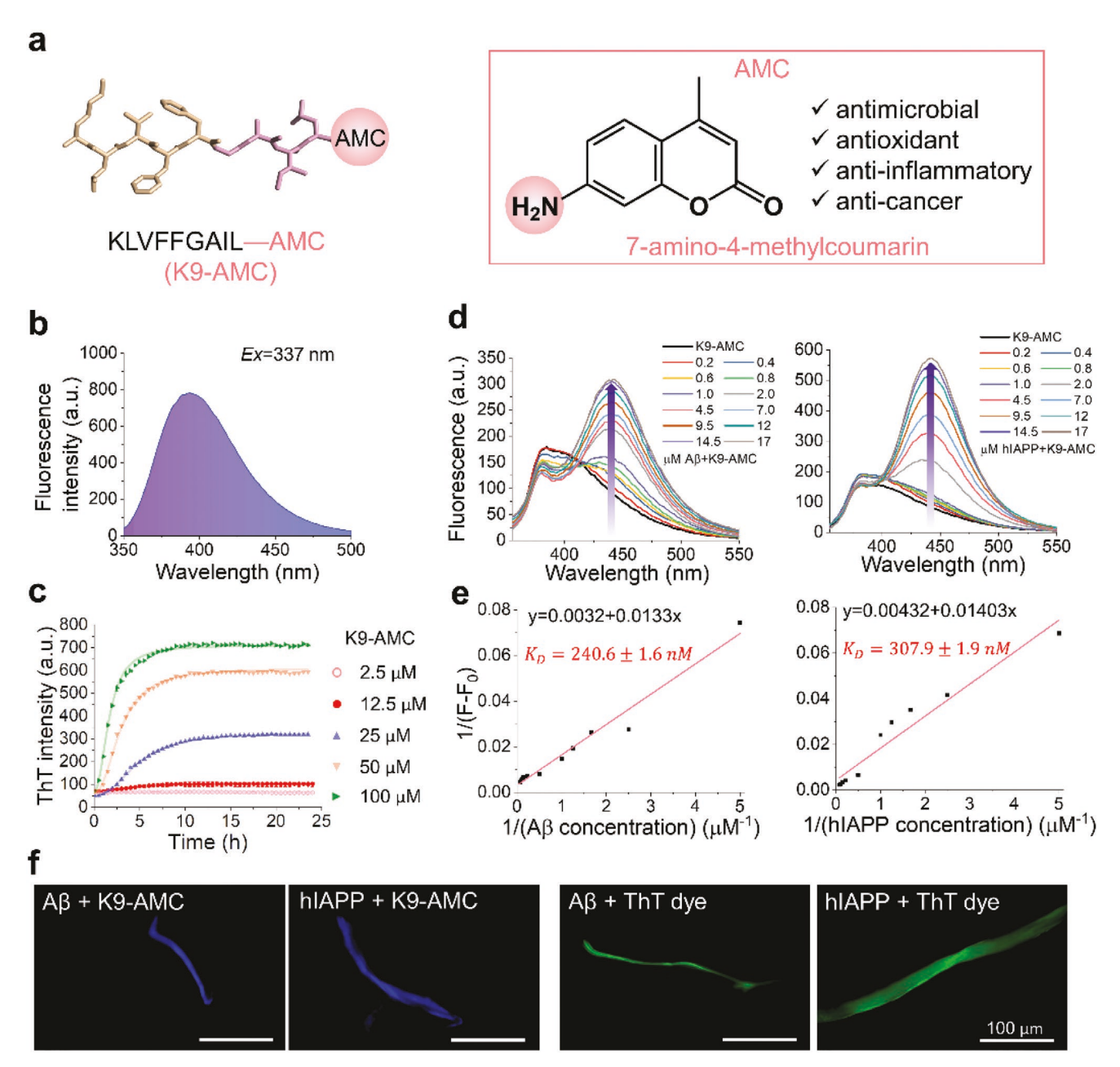


Figure 3. Fluorescent and self-aggregation properties of K9-AMC. a) Design of K9-AMC by conjugating aromatic 7-amino-4-methylcoumarin (AMC) to C-terminal of K9 peptide for introducing the enhanced hydrophobic and π - π interactions with amyloid peptides. b) Fluorescence emission of K9-AMC at a concentration of 0.5 μM under the excitation of 355 nm. c) Self-aggregation of K9-AMC in a concentration-dependent manner by ThT fluorescence assay. d) K9-AMC (0.2 μM) fluorescence emission as the increased concentrations of A β and hIAPP. e) Binding affinity (K_D) of K9-AMC to freshly prepared A β and hIAPP using fluorescence titration. f) Representative fluorescence microscopy images of A β and hIAPP fibrils in K9-AMC (10 μM) and ThT (10 μM) solutions.

transition from disordered structures to β -sheet-rich assemblies after 24 h (Figure S4c, Supporting Information), similar to the conformational change of pure hIAPP. But the entire structural transition of hIAPP was delayed by K9-AMC at all timepoints (Figure 4b). Further deconvolution of CD spectra showed the decreased β -sheet content being proportional to the amount of K9-AMC, with a maximum of 31.6% of β -sheet reduction as compared to pure A β and 12.0% of β -sheet reduction as compared with pure hIAPP (Figure 4c). AFM images in

Figure 4d showed that both $A\beta$ and hIAPP assembled into long and dense fibrillar aggregates after 24 h. Differently, the equimolar incubation of K9-AMC with $A\beta$ can greatly suppressed amyloid fibril formation, resulting in spherical aggregates and short fibrils. Such inhibition efficacy became more pronounced when adding 4 molar excess of K9-AMC to $A\beta$ solution, leading to only several spherical aggregates being formed. Similarly, the increasing amount of K9-AMC reduced the formation of hIAPP fibrils. All anti-aggregation data from ThT, AFM,

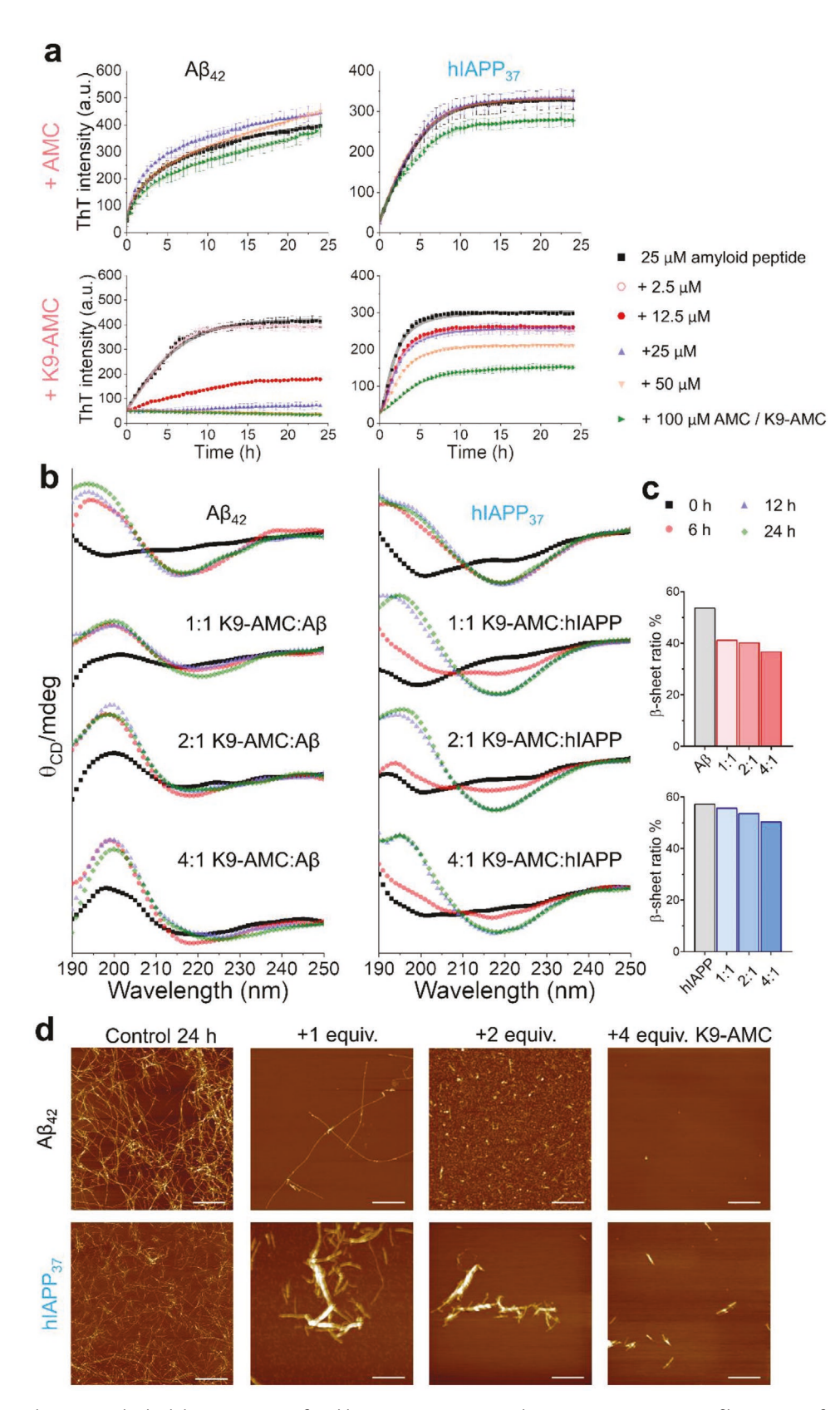


Figure 4. K9-AMC enhances amyloid inhibition against A β and hIAPP aggregation. a) ThT Kinetic aggregation profiles to quantify the inhibition of A β (25 μM) or hIAPP (25 μM) in the absence (black) or presence of AMC and K9-AMC at different concentrations (2.5–100 μM). All data represent mean \pm standard error of triplicate measurements. b) CD spectra of A β (25 μM) or hIAPP (25 μM) in the absence and presence of 1, 2, and 4 molar equivalent





www.afm-journal.de

and CD confirm the interaction-induced inhibition ability of K9-AMC to redirect the assembly of amyloid peptides, retard the amyloid fibrillization, and disfavors the fibril elongation.

2.3. K9-AMC Modulates Amyloid Toxicity and Antimicrobial Activity

Inhibition of amyloid aggregation does not necessarily lead to the reduction of amyloid toxicity. Here, we applied MTT assays to examine whether K9-AMC could protect both SH-SY5Y and rat RIN-5fm cells from A β - and hIAPP-induced toxicity within 24 h. While K9-AMC exhibited self-aggregation property at 25 μM or above (Figure 3c), K9-AMC aggregates were nontoxic to SH-SY5Y cells. On the contrary, RIN-5fm cells were highly susceptible to K9-AMC, which decreased cell viability to 73.0-88.9% at 25-100 µM for 24 h (Figure 5a). Co-incubation of K9-AMC with $A\beta$ in SH-SY5Y cell culture led to the dosedependent protection on A β -induced cytotoxicity, in which cell viability was increased from 63.6% to 75.4% as a K9-AMC:A β ratio increased from 1:1 to 4:1. This is consistent with the inhibition effect of K9-AMC on A β aggregation, indicating that inhibition of A β aggregation by K9-AMC also allows to reduce $A\beta$ -induced cell toxicity. However, K9-AMC offered the limited benefits to hIAPP-induced cytotoxicity, as evidenced by cell viability of 54.4%, 54.5%, 63.3%, and 60.3% in the presence of 0, 25, 50, 100 μM of K9-AMC, respectively. K9-AMC only at 100 µM improved the cell viability by 10% with significant difference (p < 0.05). It appears that the cytotoxicity of K9-AMC to RIN-5fm cells corresponds to the degree of possible oligomerization, which is likely associated with its specific structure and interactions with hIAPP. More fundamentally, hybrid APFamyloid aggregates formed by APFs (KLVFF, FGAIL, K9, and K9-AMC) and amyloid peptides (A β and hIAPP) might have a wide structural and functional diversity along the complex co-assembly pathways. Some hybrid aggregates might initiate the apoptosis pathway and they are extremely toxic, while the others are possibly off-pathway species that proceed to the fibril formation or are deposited into inclusion bodies. The less cell protection role of FGAIL or K9 in RIN-m5F could be due to the lack of membrane-anchoring residues in our APF design. Specifically, FGAIL was selected from the core amyloidogenic region (residues 23-27) located at the turn and near to C-terminal region of hIAPP, whose major function is to inhibit the folding and aggregation of hIAPP. It is well-known that N-terminal region of hIAPP (particular residues 1-19) is responsible for the cell membrane anchoring, binding, and penetrating, [51,52] thus lack of these membrane binding residues/sequences in FGAIL and K9 likely contributes to their weak interactions with cell membranes, [53,54] leading to the less cell protection effect on RIN-m5F cells even both APFs

possessed strong ability to inhibit the aggregation of hIAPP in bulk solution.

Considering that i) microbe-induced neuroinflammation is considered as a potential risk factor to trigger the pathologies of PMDs^[55–58] and ii) AMC possesses an intrinsic antibacterial property, we examined the antimicrobial activity of amyloid proteins, K9, AMC, and K9-AMC against both representative Grampositive (S. aureus and S. epidermidis) and Gram-negative (E. Coli and P. aeruginosa) bacteria using optical absorbance (600 nm) measurement. In contrast to the mild influence on Gram-negative bacteria (E. Coli and P. aeruginosa) growth (Figure S6, Supporting Information), the effective inhibition effects of amyloid proteins, K9, AMC, and K9-AMC on Gram-positive (S. aureus and S. epidermidis) were observed. This is not surprising because different from Gram-positive pathogens with single-layer cell membrane, Gram-negative pathogens have an extra outer layer in their cell membranes, which functions not only as physical barriers for cell entry, but also as powerful molecular efflux pumps to clear any antibiotics from the cells.^[59] It is likely that our AFPs do not contain strong cell-penetration sequences/residues to penetrate into the cell membrane of Gram-negative bacteria, thus further engineering of the AFPs in the future work is considered to include antimicrobial peptides or cell-penetrating peptides into AFP sequences for enhancing their cell-penetrating properties. The bacteria growth profiles in Figure S5a,d, Supporting Information showed that K9 at 25 µM or above exhibited limited reduction effect on S. aureus growth by 25%, but K9 at increasing concentrations of 25-250 µM reduced S. epidermidis growth by 23-64%. However, AMC at the concentrations of 5-250 µM did not influence the growth of both S. aureus and S. epidermidis (Figure S5b,e, Supporting Information). K9-AMC (250 µM) exhibited improved antibacterial activity against S. aureus and S. epidermidis growth by 42% and 67%, respectively (Figure S5c,f, Supporting Information). [60,61] Upon the confirmation of antibacterial activity of K9-AMC, we further investigated whether the co-incubation of K9-AMC with $A\beta$ or hIAPP and their as-formed complexes could possess similar antibacterial efficiency, relative to that of pure $A\beta$ and hIAPP. As shown in Figure 5b,c, both A β and hIAPP alone (25 μ M) exhibit the modest inhibition against the growth of S. aureus (69.7% with $A\beta$ and 84.0% with hIAPP), but not that of S. epidermidis (107.6% with $A\beta$ and 93.0% with hIAPP). Remarkably, the addition of 100 μ M K9-AMC to either A β or hIAPP significantly increased the overall antimicrobial activity against both bacteria. Specifically, A β /K9-AMC reduced the bacterial density of *S. aureus* and S. epidermidis by 49% and 31%, while hIAPP/K9-AMC also inhibited the bacterial density of S. aureus and S. epidermidis by 32% and 51%. Different antimicrobial activities of amyloid/K9-AMC complexes probably imply different complex interplays of the sequence-structure-interaction between K9-AMC and amyloid in the context of cell membranes.

K9-AMC. To rule out the background influence of strong CD signals from native K9-AMC, CD spectra are reorganized by subtracting the background K9-AMC signals in Figure S4a, Supporting Information, from the whole CD signals of A β and hIAPP with K9-AMC in Figure S4b,c, Supporting Information. c) Final β -sheet structure contents of A β and hIAPP in the absence and presence of K9-AMC after 24 h incubation. d) AFM images of A β (25 μ M) or hIAPP (25 μ M) aggregates in the absence or presence of 1, 2, and 4 molar equivalent K9-AMC. All samples are imaged after 24 h incubation under physiological conditions (pH 7.4, 37 °C). Scale bars = 1 μ m.

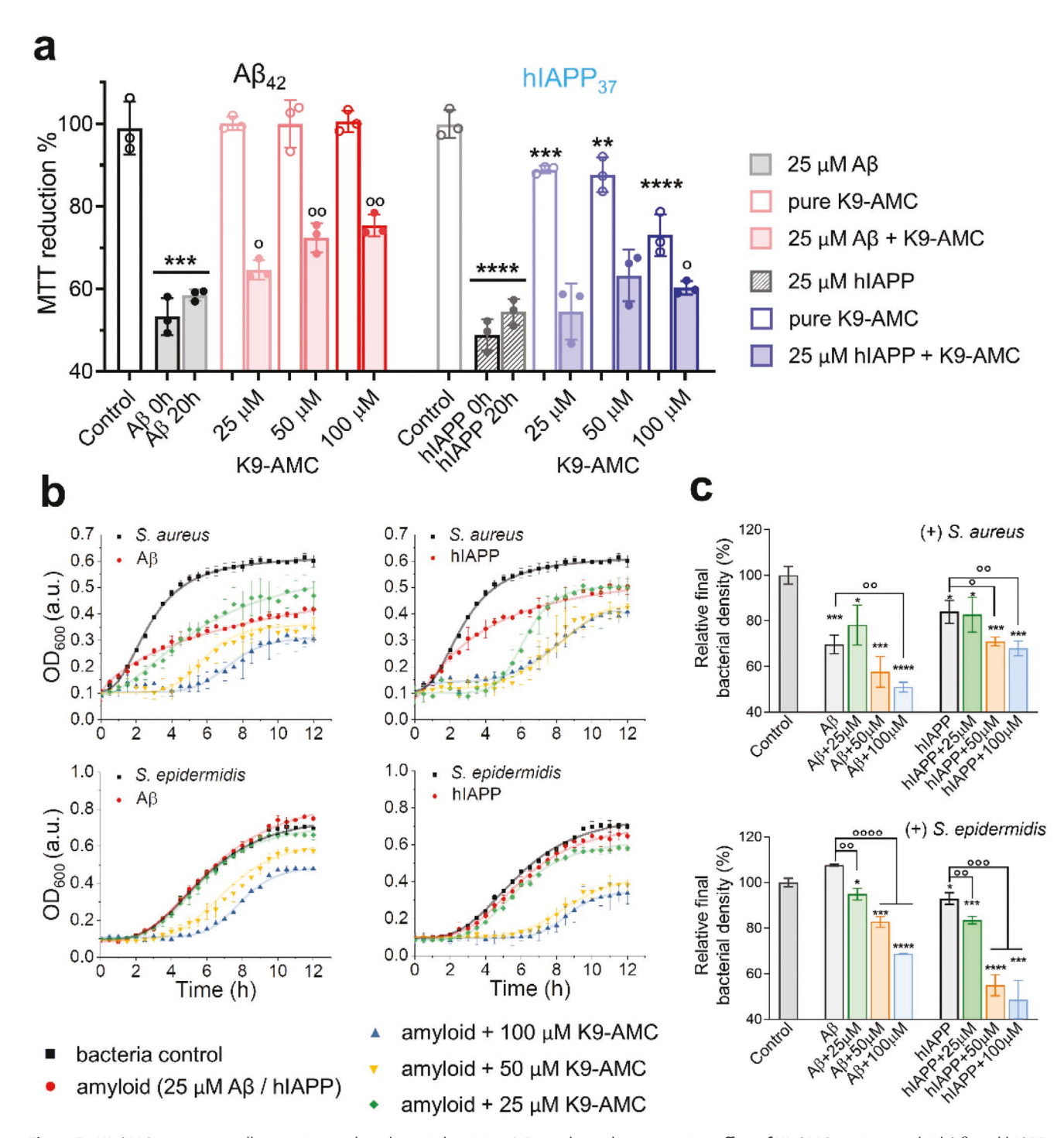


Figure 5. K9-AMC possesses cell protection and antibacterial activity. a) Dose-dependent protection effect of K9-AMC against amyloid A β - and hIAPP-induced cellular toxicity by MTT assay. b) Statistical analysis (n=3) is conducted for cells/bacteria treated with K9-AMC, A β , or hIAPP alone relative to control (*, p < 0.05; ***, p < 0.01; ****, p < 0.001; ****, p < 0.001) as well as cells/bacteria treated with both K9-AMC and A β or hIAPP relative to cells/bacteria treated with A β or hIAPP alone (°, p < 0.05; °°, p < 0.001; °°°, p < 0.001; °°°, p < 0.001).

3. Conclusions

In this study, we proposed a step-by-step strategy to rationally design new APFs and APFs-fluorescent conjugates with β -structure-forming property, which serve as multi-target

amyloid inhibitors to prevent both amyloid aggregation of $A\beta$ and hIAPP and microbial infection of S. aureus and S. epidermidis. Through a step-by-step design, the original APFs of KLVFF from $A\beta$ and FGAIL from hIAPP—capable of forming β -structure-rich amyloid-like fibrils—were first engineered by



FUNCTIONAL

www.afm-journal.de

combing both KLVFF and FGAIL into a single KLVFFGAIL (K9). The hybrid sequence of K9 allowed to promote the crossinteractions with both $A\beta$ and hIAPP, which in turn introduced a new dual inhibition function to prevent A β and hIAPP fibrillization by 97% and 39% and to reduce A β - and hIAPPinduced cell toxicity by 58% and 5%. Next, AMC as an antimicrobial fluorescence was conjugated to K9 to produce K9-AMC. The resultant K9-AMC exhibited high nanomolar binding affinity of 240.6 \pm 1.6 nM and 307.9 \pm 1.9 nM to A β and hIAPP, respectively. Consequently, the strong binding affinity between K9-AMC and amyloid peptides led to the higher amyloid inhibition property by the reduction of $A\beta$ and hIAPP fibrils up to 100% and 56% and the increase of cell viability by 10-32% at optimal conditions. As compared to K9, the enhanced amyloid inhibition property of K9-AMC is likely stemmed from the AMC, whose hydrophobic, aromatic nature allows to interact strongly with amyloid peptides to disturb amyloid structural transition, reduce β -structure content, and block aggregation pathways. More importantly, the antimicrobial nature of AMC in K9-AMC also introduced a new and strong antimicrobial activity against the growth of S. aureus and S. epidermidis by ≈40-70%. This work provides a general design strategy by selecting, engineering, and optimizing APFs and functional APF-conjugates, which can serve as dual-/multi-target inhibitors to suppress amyloid aggregation and microbial infection simultaneously for achieving more pharmaceutical/clinical effectiveness for amyloid disease treatments.

4. Experimental Section

Materials: A β (1-42) and hIAPP (1-37) was purchased from the CPC Scientific (San Jose, CA), short peptide sequence, including KLVFF, FGAIL, KLVFFGAIL, and C-terminal modified KLVFGAIL-AMC were from GenScript (Piscataway, NJ), AMC (7-amino-4-methylcoumarin) was from BeanTown Chemical (Hudson, NH). HFIP (1,1,1,3,3,3-Hexafluoro-2-propanol), DMSO (dimethyl sulfoxide), and ThT (thioflavine T) were from Sigma-Aldrich (St. Louis, MO).

Preparation of Monomeric Peptide Solutions: Peptides (lyophilized powder, 1 mg) were dissolved in 1 mL HFIP and sonicate for 30 min on ice, followed with 30 min centrifugation (14 000 rpm, 4 °C), to obtain homogeneous, aggregate-free peptide solution. The supernatants were aliquoted and lyophilized to remove solvent. Peptides were first gradually dissolved in 10 mM NaOH (KLVFGAIL-AMC in 5% acetic acid) with gentle tapping, and further diluted in buffer (PBS, 10 mM, pH 7.4) to final concentration.

Thioflavin T (ThT) Fluorescence Assay: ThT stock solutions were prepared by dissolving 2 mM ThT in 10 mM Tris buffer solution (pH = 7.4) and then filtering through 0.2 μ m filter. ThT stock solution was further diluted to final concentration of 10 μ M Tris buffer before fluorescence assay. The peptides were diluted in ThT solution to desired concentrations and each was measured with three identical 200 μ L samples. The amyloid growth kinetics were measured by SpectraMax M3 microplate reader (Molecular Devices, CA, USA), at excitation wavelength of 450 nm and emission wavelength at the range of 470 to 500 nm under kinetic bottom-read mode. Measurements were taken every 30 min at 37 °C incubation.

CD Spectroscopy: Secondary structure change of peptides was monitored for 3 days at 37 °C. Samples were prepared by dissolving amyloid peptides in 10 mM sodium phosphate buffer (pH = 7.4) and incubated at 37 °C. After different time intervals, aliquot of sample solution was measured in a quartz cell with 1 mm path length. The CD spectra of peptide solutions were measured using J-1500 spectropolarimeter (Jasco Inc., Japan) and scanned between 190 and

250 nm with a step size of 0.5 and 50 nm $\rm min^{-1}$ scan rate. The secondary structures were predicted by using the Beta Structure Selection (BeStSel) algorithm.^[62]

Atomic Force Microscopy (AFM): Morphology of amyloid aggregates with or without the inhibitors was observed using Nanoscope MultiMode 8 AFM (Bruker, NY, USA). 20 μ L amyloid solution was deposited on mica surface and rinsed with water to remove salts. The as-prepared samples were blotted and subsequently imaged by silicon AFM probe with a nominal radius of <10 nm and 150 kHz resonant frequency (Aspire, USA), in tapping mode with a scan rate of 1.0 Hz.

Fluorescence Microscopy: The fluorescent signals of K9-AMC and Aβ/hIAPP co-incubated with K9-AMC were detected by fluorescence microscope Olympus IX81 (Olympus, Japan). 25 μM Aβ/hIAPP were incubated in 10 mM sodium phosphate buffer (pH 7.4) at 37 °C for 24 h to form mature fibrillar aggregates. Freshly prepared K9-AMC or ThT stock solution (2 mM in 10 mM PBS buffer) were added into the aged Aβ/hIAPP solution to reach a final concentration of 10 μM, and co-incubated for 10 min before fluorescence microscope imaging. As a control, AMC (10 μM) was added into the aged Aβ/hIAPP fibril solution for 10 min before fluorescence microscope imaging. And the pure K9-AMC fibrils were prepared at concentration of 1 mM in PBS buffer for incubating under 37 °C for 48 h and imaged with or without 10 μM ThT dve.

Fluorescence Titrations: Fluorescence titration studies were performed using LS 55 Fluorescence Spectrometer (PerkinElmer, USA) and measured in 3 mL quartz cuvette. The excitation wavelength was fixed at 337 nm (slit width: 10 nm) and emission spectra were collected between 350–550 nm (slit width: 7.5 nm). The apparent binding constant $K_{\rm D}$ of the interaction between K9-AMC with A β /hIAPP were quantified by titrating K9-AMC (200 nM) with increasing amount of A β /hIAPP. In detail, for all experiments, freshly prepared 200 nM K9-AMC in 10 mM sodium phosphate buffer (pH 7.4) was allowed to equilibrate for 2 min before recorded and titrated with freshly prepared A β /hIAPP solutions. The fluorescence spectra of K9-AMC were tested with increasing concentrations of ligand A β /hIAPP from 0 to 17 μ M. Control buffer titration was also performed in parallel for diminishing background influence in each experiment. Data were analyzed using

1:1 binding model $(\overline{F_t} - \overline{F_0}) = \overline{F_{max}} - \overline{F_0}^+ \overline{F_0} + \overline{F_0}$ where F_t is the fluorescence intensity during titration, F_0 is the fluorescence intensity before titration, F_{max} is the maximum fluorescence intensity, [X] is the ligand concentration, and K_D is the equilibrium binding constant) and were means (\pm SD) of three binding curves.

Cell Viability Assay: The cytotoxicity of amyloid peptides and the effect of inhibitors on the amyloid-induced cytotoxicity was examined by in vitro MTT assay. Human neuroblastoma SH-SY5Y cells (ATCC CRL-2266, VA, USA) and the rat insulinoma cells RIN-m5F (ATCC CRL-11605, VA, USA) were chosen for examining A β - and hIAPP-induced cytotoxicity, respectively. SH-SY5Y cells were cultured in 1:1 Eagle's minimum essential medium (EMEM)/Ham's F-12 medium (F12), and RIN-m5F cells were cultured in RPMI-1640 medium. All culture mediums were supplemented with 10% fetal bovine serum and 1% penicillin/ streptomycin. The cells were incubated at 37 °C in 5% CO2 humidified incubator and separately seeded onto 96-well plate (104 cells in 100 µL) after reaching over 80% confluence. After incubated for 24 h, the medium was replaced with fresh medium containing amyloid peptides. The cells were further incubated for 24 h, followed by replacing the medium with 0.5 mg mL⁻¹ 3-(4,5-dimethylthiazole-2-yl)-2,5-diphenyltetrazolium bromide (MTT) solution and incubated for another 4 h. The culture medium was replaced by dimethyl sulfoxide to dissolve the formazan crystals formed through MTT reduction in cells. The absorbance value was read at 540 nm, and the cell viability was determined as the percentage of MTT reduction as compared to untreated cells. Data were exhibited in mean±s.d. of three independent tests.

Bacterial Growth Assays: S. aureus (ATCC 6538P) and S. epidermidis (ATCC 14 990) were grown to late-lag phase and diluted to an OD_{600} value of 0.05. Peptides at desired concentration were added in experimental groups and the growth curves of bacteria were recorded by measuring the OD_{600} in the following 12 h at 37 °C by microplate reader



FUNCTIONAL MATERIALS www.afm-journal.de

(SpectraMax M3). The final bacterial density after the addition of each peptide and their complexes was compared relative to that of untreated control (100% bacterial density).

Supporting Information

Supporting Information is available from the Wiley Online Library or from the author.

Acknowledgements

Y.Z. and Y.T. contributed equally to this work. The authors thank financial support from NSF-2107619.

Conflict of Interest

The authors declare no conflict of interest.

Data Availability Statement

Research data are not shared.

Keywords

Alzheimer disease, amyloid proteins, antimicrobial activity, protein aggregation, type 2 diabetes

Received: March 27, 2021 Revised: April 25, 2021 Published online:

- Y. Zhang, M. Zhang, Y. Liu, D. Zhang, Y. Tang, B. Ren, J. Zheng, J. Mater. Chem. B 2021, 9, 3300.
- [2] B. Ren, Y. Liu, Y. Zhang, M. Zhang, Y. Sun, G. Liang, J. Xu, J. Zheng, J. Mater. Chem. B 2018, 6, 56.
- [3] B. Ren, Y. Liu, Y. Zhang, Y. Cai, X. Gong, Y. Chang, L. Xu, J. Zheng, ACS Chem. Neurosci. 2018, 9, 1215.
- [4] K. Bourgade, H. Garneau, G. Giroux, A. Y. Le Page, C. Bocti, G. Dupuis, E. H. Frost, T. Fülöp, Biogerontology 2015, 16, 85.
- [5] D. A. Green, E. Masliah, H. V. Vinters, P. Beizai, D. J. Moore, C. L. Achim, Aids 2005, 19, 407.
- [6] M. Karpenko, Z. Muruzheva, N. Pestereva, I. Ekimova, Neurosci. Behav. Physiol. 2019, 49, 555.
- [7] M. J. Krysmann, V. Castelletto, A. Kelarakis, I. W. Hamley, R. A. Hule, D. J. Pochan, *Biochemistry* 2008, 47, 4597.
- [8] K. Tenidis, M. Waldner, J. Bernhagen, W. Fischle, M. Bergmann, M. Weber, M.-L. Merkle, W. Voelter, H. Brunner, A. Kapurniotu, I. Mol. Biol. 2000, 295, 1055.
- [9] P. Friedhoff, J. Biernat, J. Heberle, E. Mandelkow, E. Mandelkow, Proc. Natl. Acad. Sci. USA 2000, 97, 5129.
- [10] M. I. Ivanova, M. R. Sawaya, M. Gingery, A. Attinger, D. Eisenberg, Proc. Natl. Acad. Sci. USA 2004, 101, 10584.
- [11] Q. Wang, G. Liang, M. Zhang, J. Zhao, K. Patel, X. Yu, C. Zhao, B. Ding, G. Zhang, F. Zhou, J. Zheng, ACS Chem. Neurosci. 2014, 5, 972.

- [12] M. A. Findeis, G. M. Musso, C. C. Arico-Muendel, H. W. Benjamin, A. M. Hundal, J.-J. Lee, J. Chin, M. Kelley, J. Wakefield, N. J. Hayward, *Biochemistry* 1999, 38, 6791.
- [13] S. M. Chafekar, H. Malda, M. Merkx, E. Meijer, D. Viertl, H. A. Lashuel, F. Baas, W. Scheper, ChemBioChem 2007, 8, 1857.
- [14] L.-M. Yan, M. Tatarek-Nossol, A. Velkova, A. Kazantzis, A. Kapurniotu, Proc. Natl. Acad. Sci. USA 2006, 103, 2046.
- [15] S. J. Soscia, J. E. Kirby, K. J. Washicosky, S. M. Tucker, M. Ingelsson, B. Hyman, M. A. Burton, L. E. Goldstein, S. Duong, R. E. Tanzi, PLoS One 2010, 5, e9505.
- [16] M. L. Gosztyla, H. M. Brothers, S. R. Robinson, Journal of Alzheimer's Disease 2018, 62, 1495.
- [17] N. B. Last, A. D. Miranker, Proc. Natl. Acad. Sci. USA 2013, 110, 6382.
- [18] Y. Hirakura, I. Carreras, J. D. Sipe, B. L. Kagan, Amyloid 2002, 9, 13.
- [19] M. Pasupuleti, M. Roupe, V. Rydengård, K. Surewicz, W. K. Surewicz, A. Chalupka, M. Malmsten, O. E. Sörensen, A. Schmidtchen, *PLoS One* 2009, 4, e7358.
- [20] M. Zhang, J. Zhao, J. Zheng, Soft Matter 2014, 10, 7425.
- [21] S. J. Soscia, J. E. Kirby, K. J. Washicosky, S. M. Tucker, M. Ingelsson, B. Hyman, M. A. Burton, L. E. Goldstein, S. Duong, R. E. Tanzi, R. D. Moir, *PLoS One* 2010, 5, e9505.
- [22] N. B. Last, A. D. Miranker, Proc. Natl. Acad. Sci. USA 2013, 110, 6382.
- [23] H. Jang, F. T. Arce, M. Mustata, S. Ramachandran, R. Capone, R. Nussinov, R. Lal, Biophys. J. 2011, 100, 1775.
- [24] B. L. Kagan, H. Jang, R. Capone, F. Teran Arce, S. Ramachandran, R. Lal, R. Nussinov, *Mol. Pharmaceutics.* **2012**, *9*, 708
- [25] H. Chu, M. Pazgier, G. Jung, S.-P. Nuccio, P. A. Castillo, M. F. de Jong, M. G. Winter, S. E. Winter, J. Wehkamp, B. Shen, N. H. Salzman, M. A. Underwood, R. M. Tsolis, G. M. Young, W. Lu, R. I. Lehrer, A. J. Bäumler, C. L. Bevins, *Science* 2012, 337, 477.
- [26] C. Code, Y. Domanov, A. Jutila, P. K. J. Kinnunen, Biophys. J. 2008, 95, 215.
- [27] J. Tian, Y. Liu, S. Miao, Q. Yang, X. Hu, Q. Han, L. Xue, P. Yang, Biomater. Sci. 2020, 8, 6903.
- [28] X. Hu, J. Tian, C. Li, H. Su, R. Qin, Y. Wang, X. Cao, P. Yang, Adv. Mater. 2020, 32, 2000128.
- [29] D. Wang, Y. Ha, J. Gu, Q. Li, L. Zhang, P. Yang, Adv. Mater. 2016, 28, 7414.
- [30] J. Gu, Y. Su, P. Liu, P. Li, P. Yang, ACS Appl. Mater. Interfaces 2017, 9, 198.
- [31] F. Panza, M. Lozupone, V. Solfrizzi, M. Watling, B. P. Imbimbo, Brain 2019, 142, 2905.
- [32] T. Fulop, J. M. Witkowski, K. Bourgade, A. Khalil, E. Zerif, A. Larbi, K. Hirokawa, G. Pawelec, C. Bocti, G. Lacombe, G. Dupuis, E. H. Frost, Front. Aging Neurosci. 2018, 10, 224.
- [33] N. Shanmugam, M. O. D. G. Baker, S. R. Ball, M. Steain, C. L. L. Pham, M. Sunde, *Biophys. Rev.* **2019**, *11*, 287.
- [34] J. Cummings, G. Lee, A. Ritter, M. Sabbagh, K. Zhong, Alzheimer's & Dementia: Translational Research & Clinical Interventions 2020, 6, e12050.
- [35] E. Andreetto, L. M. Yan, M. Tatarek-Nossol, A. Velkova, R. Frank, A. Kapurniotu, Angew. Chem., Int. Ed. 2010, 49, 3081.
- [36] A. Kapurniotu, Nat. Struct. Mol. Biol. 2020, 27, 1006.
- [37] T. M. Costa, L. B. B. Tavares, D de Oliveira, Appl. Microbiol. Biotechnol. 2016, 100, 6571.
- [38] X. Liu, M. Dong, X. Chen, M. Jiang, X. Lv, J. Zhou, Appl. Microbiol. Biotechnol. 2008, 78, 241.
- [39] Y. Bai, D. Li, T. Zhou, N. Qin, Z. Li, Z. Yu, H. Hua, J. Funct. Foods 2016. 20. 453.
- [40] A. Thakur, R. Singla, V. Jaitak, Eur. J. Med. Chem. 2015, 101, 476.
- [41] Y. Zhang, Y. Tang, D. Zhang, Y. Liu, J. He, Y. Chang, J. Zheng, Chin. J. Chem. Eng. 2021, 30, 225.



____MATERIALS

www.advancedsciencenews.com www.afm-journal.de

- [42] C. Röder, T. Kupreichyk, L. Gremer, L. U. Schäfer, K. R. Pothula, R. B. Ravelli, D. Willbold, W. Hoyer, G. F. Schröder, *Nat. Struct. Mol. Biol.* 2020, 27, 660.
- [43] P. T. Nguyen, X. Zottig, M. Sebastiao, S. Bourgault, Biochemistry 2017, 56, 3808.
- [44] X. M. Liu, Q. Zhao, W. C. Song, X. H. Bu, Chem. Eur. J. 2012, 18, 2806.
- [45] J. Molina-Bolívar, F. Galisteo-González, C. C. Ruiz, M. Medina-O'Donnell, A. Martínez, A. Parra, Spectrochim. Acta, Part A 2019, 214, 161.
- [46] S. Zhang, K. I. Assaf, C. Huang, A. Hennig, W. M. Nau, Chem. Commun. 2019, 55, 671.
- [47] P. Thordarson, Chem. Soc. Rev. 2011, 40, 1305.
- [48] G. Manzo, M. A. Scorciapino, P. Wadhwani, J. Bürck, N. P. Montaldo, M. Pintus, R. Sanna, M. Casu, A. Giuliani, G. Pirri, V. Luca, A. S. Ulrich, A. C. Rinaldi, *PLoS One* 2015, 10, e0116379.
- [49] M. Migliore, A. Bonvicini, V. Tognetti, L. Guilhaudis, M. Baaden, H. Oulyadi, L. Joubert, I. Ségalas-Milazzo, Phys. Chem. Chem. Phys. 2020, 22, 1611.
- [50] S. Brahms, J. Brahms, J. Mol. Biol. 1980, 138, 149.
- [51] J. R. Brender, E. L. Lee, M. A. Cavitt, A. Gafni, D. G. Steel, A. Ramamoorthy, J. Am. Chem. Soc. 2008, 130, 6424.

- [52] J. R. Brender, K. Hartman, K. R. Reid, R. T. Kennedy, A. Ramamoorthy, *Biochemistry* 2008, 47, 12680.
- [53] D. C. R. Camargo, D. Garg, K. Buday, A. Franko, A. R. Camargo, F. Schmidt, S. J. Cox, S. Suladze, M. Haslbeck, Y. G. Mideksa, *Chem. Commun.* 2018, 54, 5426.
- [54] M. Zhang, B. Ren, Y. Liu, G. Liang, Y. Sun, L. Xu, J. Zheng, ACS Chem. Neurosci. 2017, 8, 1789.
- [55] T. Wyss-Coray, Nat. Med. 2006, 12, 1005.
- [56] M. T. Heneka, M. J. Carson, J. El Khoury, G. E. Landreth, F. Brosseron, D. L. Feinstein, A. H. Jacobs, T. Wyss-Coray, J. Vitorica, R. M. Ransohoff, *Lancet Neurol.* 2015, 14, 388.
- [57] H. Tilg, A. R. Moschen, Gut 2014, 63, 1513.
- [58] C. Ohlsson, K. Sjögren, Trends Endocrinol. Metab. 2015, 26, 69.
- [59] J. Costerton, J. Ingram, K. Cheng, Bacteriol. Rev. 1974, 38, 87.
- [60] M. Dathe, T. Wieprecht, H. Nikolenko, L. Handel, W. L. Maloy, D. L. MacDonald, M. Beyermann, M. Bienert, FEBS Lett. 1997, 403, 208.
- [61] Y. Rosenfeld, N. Lev, Y. Shai, Biochemistry 2010, 49, 853.
- [62] A. Micsonai, F. Wien, L. Kernya, Y.-H. Lee, Y. Goto, M. Réfrégiers, J. Kardos, Proc. Natl. Acad. Sci. USA 2015, 112, E3095.